energy&fuels

pubs.acs.org/EF

Article

Occurrence Space and State of Petroleum in Lacustrine Shale: Insights from Two-Step Pyrolysis and the N_2 Adsorption Experiment

Yuping Wu, Chenglin Liu,* Fujie Jiang,* Tao Hu, Rizwan Sarwar Awan, Zhangxin Chen, Jiahao Lv, Chenxi Zhang, Meiling Hu, Renda Huang, and Guanyun Wu

Cite This: *Energy Fuels* 2022, 36, 10920−10933

Read Online

ACCESS | Metrics & More | Article Recommendations

ABSTRACT: The pore structure and occurrence state of hydrocarbons in shale reservoirs are significant factors affecting shale oil production. However, how pore structure affects the occurrence of shale oil remains unclear. This paper aims at analyzing the major distribution space of shale oil with various physical states in shale pores using experimental approaches. Therefore, the original samples and solvent-extracted samples of lacustrine shale from the Permian Fengcheng Formation in Junggar Basin were investigated using X-ray diffraction (XRD), field emission scanning electron microscopy (FE-SEM), Rock-Eval pyrolysis, and N_2 adsorption/desorption methods. The findings demonstrate that the Fengcheng shale has high oil content, with free oil accounting for 57.17% of the total oil yield. The pore size distribution characteristics of original and solvent-extracted shale samples indicate that shale oil is mainly stored in mesopore pores with diameters between 5 and 40 nm. The threshold limit of pore diameter for the movable oil in shale reservoirs is between 3.5 and 19 nm. Also, by comparing shale oil mobility in various basins, it is found that petroleum mobility occurs when the total oil yield in the shale reaches 6 mg HC/g Rock. Meanwhile, the threshold value of petroleum mobility in different basins is related to the pore shape. Parallel plate pores within shales are more favorable for petroleum mobility. This research presents the mobility of the shale oil threshold, which is critical for shale oil exploration and exploitation.

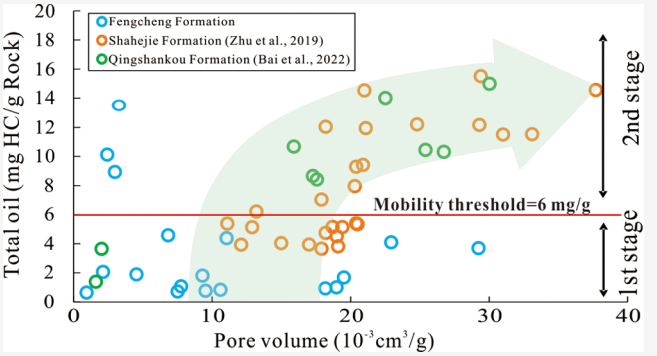

1. INTRODUCTION

Shale oil is becoming more important in the global energy landscape as conventional petroleum production declines and unconventional resource production rises fast.[1−5] Unlike conventional petroleum, shale oil refers to the in-situ and/or migrated oil resources in organic-rich shale and adjacent low-total organic carbon (TOC) reservoirs.[6,7] Meanwhile, shale is a complex mixture of inorganic minerals and organic matter (OM).[8,9] Thus, the composition of inorganic minerals and the characteristic of OM are important for the development of pore and fracture in shale systems.[10−12] The organic-rich shale does not generate oil and gas until it reaches thermal maturity. As the amount of hydrocarbons produced becomes sufficient for kerogen adsorption and fills the OM pores, the hydrocarbons start to migrate to other pore spaces in the shale reservoir.[13,14] In addition to the external geological factors such as temperature and pressure, the physical properties of liquid hydrocarbons are determined by both OM and inorganic minerals.[15] Meanwhile, the thermal maturity of OM and the formation of hydrocarbons in shale reservoirs will inevitably change the pore structure of shale, thus affecting the measurement results of pores by traditional experiment methods.[14,16,17] However, there is a scarcity of quantitative studies on the distribution of shale oil in various physical states and pore sizes.[16,18−23] To overcome this issue, it is vital to precisely characterize the pore size distribution (PSD), determine the petroleum occurrence state, and link them spatially.

CO_2 and N_2 adsorption/desorption, mercury intrusion porosimetry (MIP), and other approaches have been widely employed to assess the pore structure of unconventional shale systems.[17,24−30] Previous studies have shown that N_2 adsorption is a good technique for evaluating mesopores with 2−50 nm diameter. In contrast, CO_2 adsorption is much more reliable in characterizing micropores with lower than 2 nm.[11,24,27,31] Additionally, the injection pressure of MIP is generally much higher (>200 MPa). Higher pressure may

Received: July 3, 2022
Revised: August 21, 2022
Published: September 2, 2022

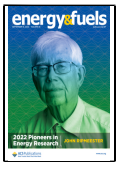

https://doi.org/10.1021/acs.energyfuels.2c02222
Energy Fuels 2022, 36, 10920−10933

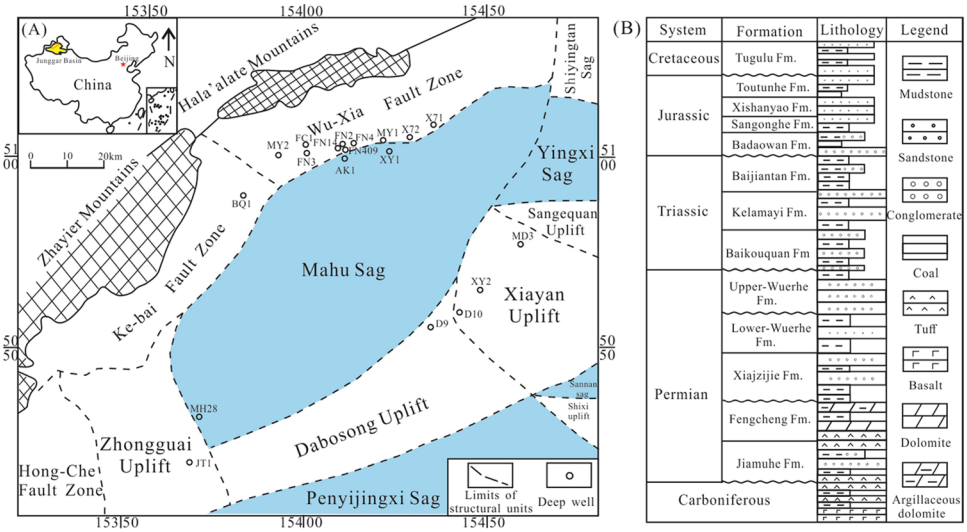

Figure 1. (A) Structural setting of the Mahu Sag, Junggar Basin; (B) stratigraphic section in the Mahu Sag (modified after Xia et al.[55]).

cause the residual hydrocarbons in the samples to move,[32] and it is also possible to produce microcracks. The tough challenge is that performing two independent MIP on the same shale sample is impossible. Furthermore, statistical study reveals that the pore size of shale is greater than 5 nm in favorable shale oil-producing areas around the world, and the distribution space of shale oil is fewer than 300 nm, accounting for more than 90% of the shale oil occurrence space.[33,34] Thus, the N_2 adsorption/desorption measurement may be the most suitable experimental method to investigate the oil distribution space in shales.

Previous studies have shown that the oil mainly occurs in two states in shale: free and adsorbed.[7,35−37] Therefore, characterizing the quantity of shale oil accurately and quantitatively in different physical states has always been a divergent scientific issue. At present, solvent extraction and pyrolysis methods are widely used to predict the physical state and the amount of hydrocarbons in liquid-rich unconventional systems.[7,38−43] Compared with solvent extraction, pyrolysis is an efficient and fast screening tool to evaluate the in-situ hydrocarbon characteristics in shale plays.[1,41,44−46] However, because of the carry-over effect, the standard pyrolysis S_1 value cannot be directly regarded as an indicator of shale oil content.[7,45,47] Its use may lead to an erroneous estimation of the quantities of hydrocarbons.[44,46] Therefore, the article that cites Jarvie's method proposed the two-step pyrolysis method, which can distinguish and evaluate oil in different physical states and has been widely cited in subsequent studies.[40,46,48−51]

This study takes lacustrine shale samples from Fengcheng Formation (P_1f) in Mahu Sag, Junggar Basin, as research objects. First, the mineral composition of shale is investigated. After that, the shale oil content and physical state were quantitatively characterized by two-step pyrolysis. Low-temperature N_2 adsorption/desorption methods are used to investigate the variation in the shale pore size before and after solvent extraction to correlate the physical state of shale oil with its distribution space. Finally, the occurrence space of petroleum and the threshold limit of the pore diameter for the movable oil are revealed, providing a foundation for unconventional petroleum exploration.

2. MATERIALS AND METHODS

The Junggar Basin is one of the important petroliferous basins in northwestern China (Figure 1A). P_1f is developed in the Mahu Sag on the northwest margin of the basin and is globally considered the oldest alkali-lacustrine source rock.[52−54] It is a semi-deep to deep lacustrine fine-grained sedimentary rock distributed over a broader area, with a maximum thickness of 1800 m (Figure 1B).[55,56] Moreover, the source rocks contain special biological types, which make the organic-rich shales have great potential for hydrocarbon generation.[52,53,57]

This study selected 18 shale samples of the P_1f at a depth of 4000−5000 m from an important well (MY1) located in the Mahu sag. Each shale sample is divided equally into two parts. The first part is retained as the original sample for measurement. The second part is extracted with an organic solvent (dichloromethane) in a Soxhlet apparatus for 7 days and then measured. X-ray diffraction (XRD), total organic carbon (TOC), Rock-Eval pyrolysis, and low-temperature N_2 adsorption/desorption procedures were used on all samples.

2.1. XRD Analysis. XRD was performed on a D2 Phaser diffractometer. About 5 g of the sample was taken, ground to 300 mesh, and smeared on a glass slide for preparation. The experimental device setting conditions were electric voltage (30 kV), electric current (10 mA), measurement range of 2θ (4.5°−50°), and sampling step width 2θ (0.02°), and each step takes 0.5 s.

2.2. TOC Determination and Rock-Eval Pyrolysis. After surface cleaning, samples were powdered to 200 meshes before for TOC and Rock-Eval pyrolysis analysis. About 0.10 g of powdered sample was used for TOC analysis. Initially, carbonate minerals were removed with 5% diluted hydrochloric acid. Then, it was washed with deionized water every half an hour, and the whole process lasted for 3 days. After drying in an oven at 110 °C, the residual organic carbon in the rock was measured by the Leco CS-230 apparatus. Pyrolysis was carried out with Rock-Eval II instrument. In the beginning, the oven was isothermally heated at 300 °C for 3 min, and the free hydrocarbon (S_1) was obtained. Then, the pyrolysis temperature was increased to 600 °C at the rate of 25 °C/min, determining the cracking hydrocarbons of kerogen (S_2) and the thermal maturity parameter (T_{max}).

2.3. N_2 Adsorption Isotherms. N_2 adsorption is an effective method to reveal the pore structure in a shale reservoir.[25] All samples were ground to a 60−80 mesh powder, and the experiments were carried out for both original and extracted samples. Before the test, the sample was dried at 110 °C for 24 h and degassed for more than 6 h. A Micromeritics ASAP 2460 instrument was used to collect data at 77 K with a relative pressure ranging from 0.005 to 0.995. According to the Brunauer−Emmett−Teller (BET) model,[58] the specific surface

https://doi.org/10.1021/acs.energyfuels.2c02222
Energy Fuels 2022, 36, 10920−10933

Table 1. Mineral Characteristics of the Studied Samples

sample no.	mineralogy (wt %)						
	quartz	K-feldspar	plagioclase	calcite	dolomite	pyrite	total clay
1	9.59	6.79	11.79	28.87	28.87	6.19	7.79
2	46.95	11.39	12.79	2.60	0.00	0.00	9.39
3	17.78	11.09	23.48	3.10	21.28	3.00	5.99
4	17.18	2.30	12.39	27.97	30.07	4.50	0.00
5	11.70	4.50	10.90	33.10	31.60	8.20	0.00
6	11.19	11.39	12.79	3.00	30.57	8.39	14.59
7	16.88	4.90	8.49	0.00	48.25	5.59	15.88
8	31.47	13.19	17.28	7.69	16.88	8.19	0.00
9	10.79	11.29	10.19	42.16	10.69	7.59	0.00
10	2.90	2.00	14.09	31.47	41.56	4.40	0.00
11	0.00	0.00	6.59	62.94	30.37	0.00	0.00
12	0.70	4.90	34.27	12.99	20.48	0.00	12.09
13	26.67	5.19	5.69	24.68	29.57	7.99	0.00
14	24.98	2.60	14.79	0.00	42.86	2.00	12.69
15	33.97	4.30	8.49	0.00	31.87	3.80	17.48
16	15.88	4.50	25.67	14.29	13.99	5.59	15.78
17	0.00	7.39	3.90	41.16	6.39	0.00	0.00
18	0.00	7.89	4.60	44.96	12.39	17.48	0.00

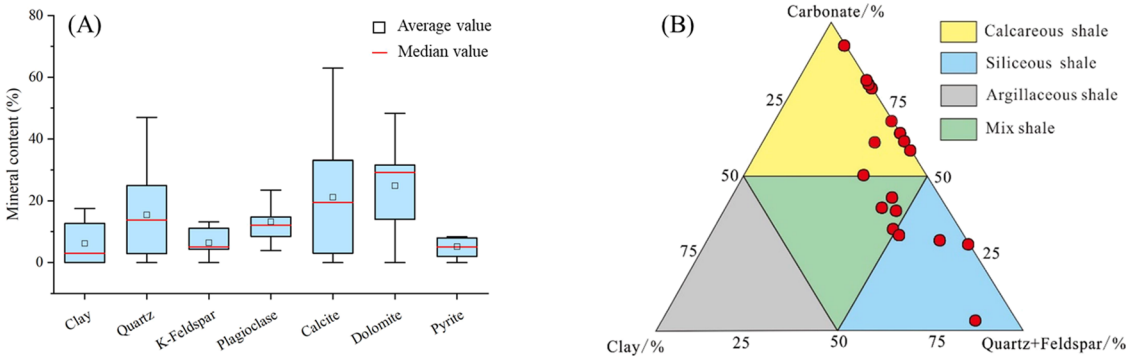

Figure 2. Mineral compositions (A) and constituents (B) of shales.

area (SSA) of the shale sample was obtained. The pore volume and pore size were obtained from the Barrett–Joyner–Halenda (BJH) model.[59] Density functional theory (DFT) was used to calculate the PSD of the sample.[60]

2.4. Field Emission Scanning Electron Microscopy. Sigma 500 SEM was used to study the microscopic pore structure of shale. The acceleration voltage of the experimental equipment was 20 keV, the magnification was up to 200,000 times, and the resolution was up to 0.8 nm. The dimension of the sample for FE-SEM imaging was a width of 10 mm, a height of 5 mm, and a length of 1.5 mm. Samples were initially polished with silicon carbide paper and then with an EM TIC 3X argon ion milling device. Before testing, the sample surfaces were gold-coated (10 nm) to improve conductivity.[61] Subsequently, the microscope is used to observe the polished surface.

3. RESULTS

3.1. Mineralogy of the Fengcheng Shale. XRD results show the studied shale samples mainly comprise the heterogenic mineral composition, that is, quartz, feldspar, dolomite, and calcite (Table 1, Figure 2A). The average quartz content is 15.48 wt %. Plagioclase and potassium feldspar account for 6.42 and 13.23 wt % of feldspar, respectively. The average content of dolomite is 24.87 wt % and that of calcite is 21.16 wt %. The clay mineral content of the samples is generally low, averaging 6.20 wt %. Pyrite is present in most of the samples, with a mean of 5.16 wt %. According to the ternary diagram, the main mineral components are carbonate (calcite + dolomite) with an average content of over 50 wt %. The other two components are clastic minerals (quartz + feldspar) and clay minerals. That is, the lithofacies of shale is mainly carbonate shale, followed by mixed shale and felsic shale (Figure 2B).

FE-SEM provides detailed mineral information on the shale samples and exhibits a variety of pore types (Figure 3). Under the electron microscope, the carbonate lamina is well developed, and the corresponding element combination reveals that it is calcite-rich laminae (Figure 3a,b). The elements such as Mg, Si, K, and Fe can be used to reflect the distributions of dolomite, felsic minerals, and pyrite (Figure 3c,d). Figure 3e shows the calcite dissolved pores, which represent intragranular dissolved pores. Clay minerals mainly develop intercrystalline micropores with an irregular morphology (Figure 3f). Cluster pyrite is often associated with OM and is easy to form abundant intercrystalline pores (Figure 3f). OM pore development is influenced by kerogen type and thermal maturation.[14,62] The organic pores in the shale are bubble-shaped or elliptic, with nanometer and micron sizes (Figure 3h). Additionally, microfractures can be observed that might be formed by compression or tectonic activity (Figure 3i), which is often used as hydrocarbon migration channels.

https://doi.org/10.1021/acs.energyfuels.2c02222
Energy Fuels 2022, 36, 10920−10933

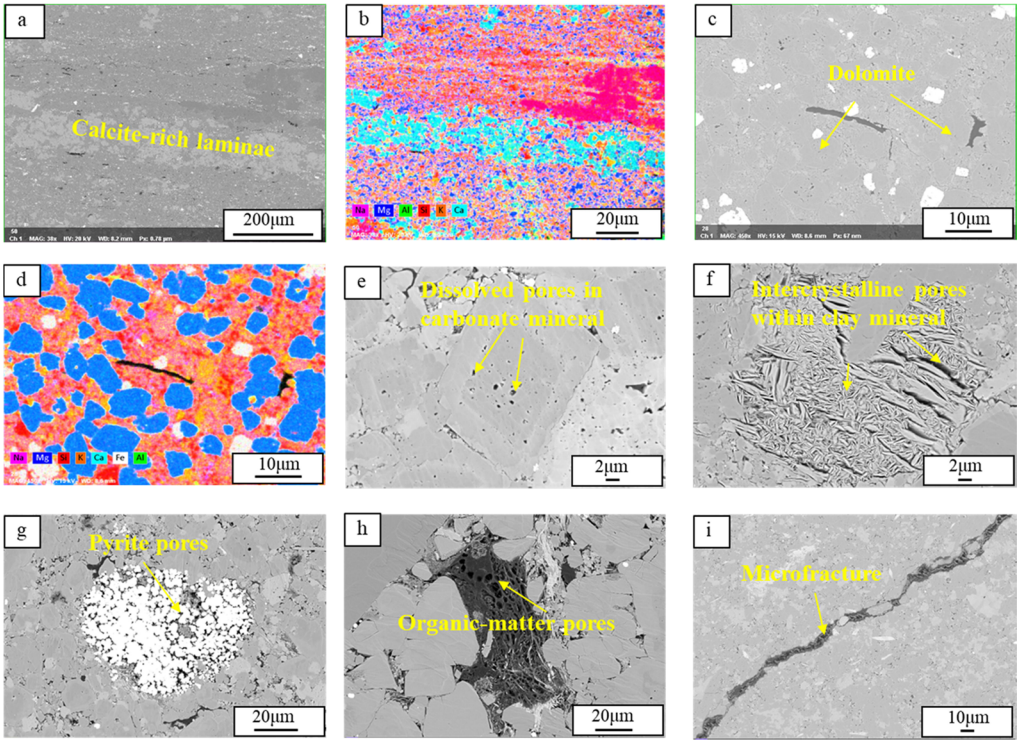

Figure 3. Representative minerals and pore types in the shale. (a) Distribution of calcite-rich lithological units; (b) major elements Mg, Ca, Al, Si, and K in image a; (c) Distribution of dolomite-rich lithological units; (d) major elements Mg, Si, and K in the image c. Element's characteristic generally indicates the dolomite; (e) dissolved pores in carbonate mineral grains; (f) intercrystalline pores within clay mineral; (g) pyrite pores; (h) organic-matter pores; (i) microfracture.

Table 2. Geochemical Characteristics of the Samples

			original sample			extracted sample		
sample no.	depth (m)	TOC (wt %)	S_1 (mg/g)	S_2 (mg/g)	T_{max} (°C)	S_1 (mg/g)	S_2 (mg/g)	T_{max} (°C)
1	4594.63	2.33	4.03	9.01	435	0.10	4.00	443
2	4910.63	1.36	8.39	5.40	421	0.02	0.25	442
3	4911.77	1.00	6.91	3.65	414	0.02	0.41	441
4	4710.99	0.94	0.60	2.48	436	0.05	1.95	440
5	4694.31	1.43	1.15	3.72	436	0.03	2.77	442
6	4772.01	1.93	0.57	12.43	445	0.04	12.31	447
7	4605.54	0.92	0.99	1.69	438	0.05	0.94	439
8	4340.00	2.31	0.39	14.69	439	0.07	14.28	442
9	4362.88	0.81	0.83	3.07	432	0.06	2.02	440
10	4527.95	0.31	0.53	0.56	418	0.05	0.26	426
11	4147.50	2.00	1.70	3.89	432	0.03	1.17	436
12	3955.58	1.02	2.48	2.55	410	0.03	0.41	430
13	4041.80	2.95	0.91	19.90	441	0.05	18.86	444
14	4082.50	2.29	1.29	4.00	434	0.04	1.15	441
15	4109.30	1.83	0.98	4.20	437	0.05	1.43	437
16	4933.50	0.41	0.74	0.47	351	0.05	0.15	429
17	5666.00	0.41	0.73	0.47	399	0.02	0.24	422
18	5667.80	0.41	0.67	0.52	401	0.04	0.31	479

3.2. Organic Geochemistry of the Original and Extracted Shale Samples. Table 2 shows the organic geochemical data of the original and solvent extracted samples. TOC in the original samples ranges from 0.31 to 2.95 wt %, averaging 1.37 wt %. S_1 varies from 0.39 to 8.39 mg/g with a mean of 1.93 mg/g. S_2 fluctuates from 0.47 to 19.90 mg/g, typically 5.15 mg/g. After extraction, S_1 and S_2 range from 0.02 to 0.10 mg/g and 0.15 to 18.96 mg/g, with an average of 0.05 mg/g and 3.54 mg/g, respectively (Figure 4A,B). The average loss rate of S_1 and S_2 is 97.4 and 32.3%, respectively (Figure 4C). For the extracted samples, the T_{max} value generally increases (Figure 4D). This is due to the carry-over effect phenomenon disappearing after solvent extraction.[45,48] The S_2 peak contains some hydrocarbons and nonhydrocarbons, resulting in lower pyrolysis peak temperatures when the S_2 peak occurs.[45,63,64]

3.3. N_2 Adsorption of the Original and Extracted Shale Samples. *3.3.1. N_2 Adsorption and Desorption*

https://doi.org/10.1021/acs.energyfuels.2c02222
Energy Fuels 2022, 36, 10920−10933

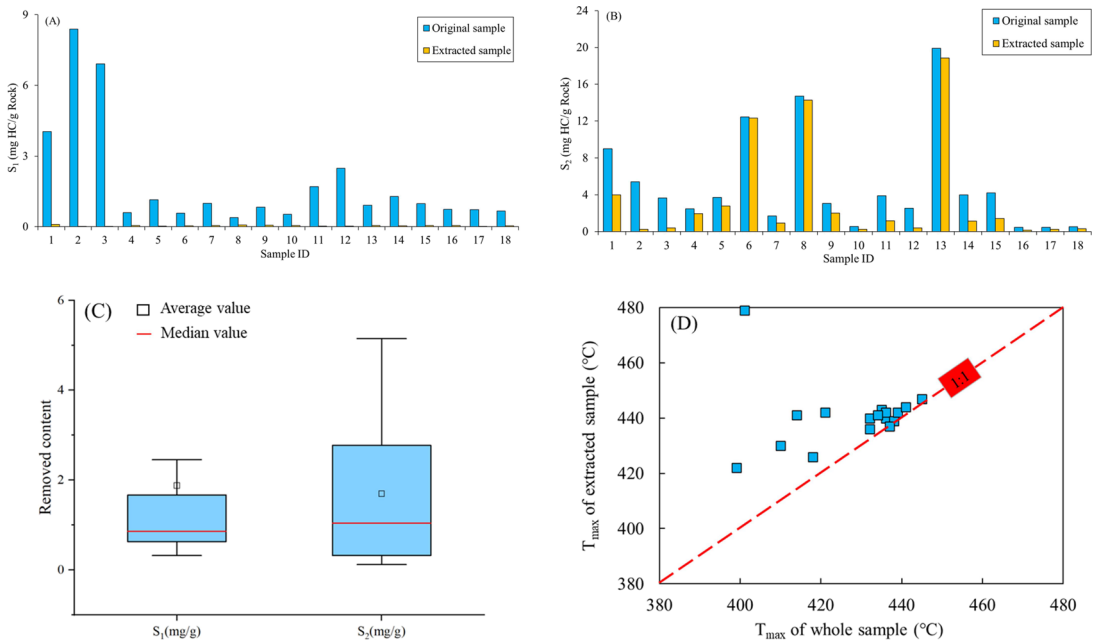

Figure 4. Graph shows the differences in geochemical data between the original and extracted samples.

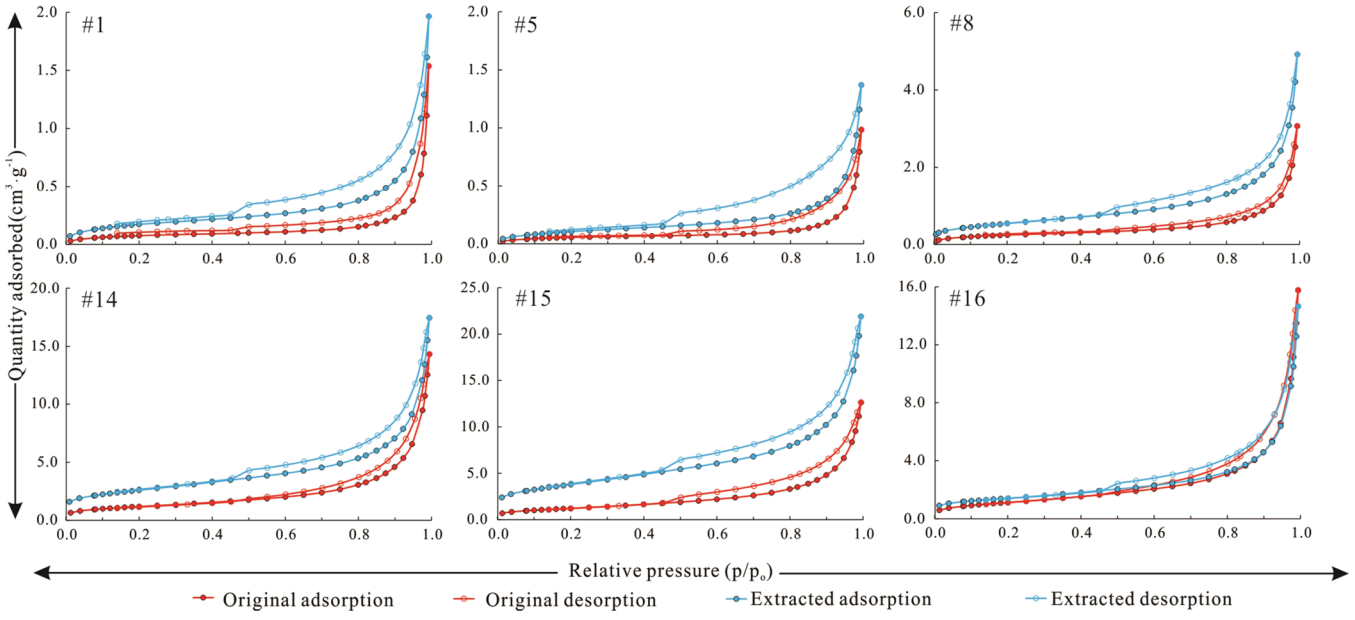

Figure 5. Representative N_2 adsorption/desorption isotherms of the original and extracted samples.

Isotherms. Figure 5 depicts the low-temperature N_2 adsorption/desorption isotherms of typical samples in this study. The combined morphology of N_2 adsorption/desorption isotherms can reflect different pore types and pore size characteristics.[26,65] The adsorption isotherms before and after solvent extraction showed an obvious hysteresis loop (P/P_o > 0.5), and there is no platform under relatively high pressure (P/P_o > 0.95). Moreover, the adsorption isotherm is almost parallel to the desorption isotherm and only increases fast when the pressure is closed to the saturated vapor pressure. It is very similar to type H3 in the IUPAC classification of the hysteresis loop, indicating that these shale samples' pores are primarily parallel plate pores.[58,66] Compared with the isotherm's characteristics of original and extracted samples, the hysteresis loop morphology of samples has no obvious change, indicating that the extraction does not affect the characteristics of the shale pore type. However, the adsorption/desorption isotherms of the extracted samples show significant uplift except for the few samples (Figure 5). In other words, under the same balance pressure, the quantity adsorbed of the extracted sample increases markedly. The adsorption capacity is closely related to the pore volume and SSA. When the pore volume and SSA increase, the adsorption capacity increases significantly.[19,65,67] When the sample is extracted by an organic solvent, the pore space originally occupied by petroleum is empty, increasing the pore volume and SSA, and thus, the quantity adsorbed.

3.3.2. SSA, Pore Volume, and Average Pore Diameter. All shale samples are statistically analyzed (Table 3 and Figure 6). The results show that the SSA of N_2-BET in the original

https://doi.org/10.1021/acs.energyfuels.2c02222
Energy Fuels 2022, 36, 10920−10933

Table 3. BET SSA, Pore Volume, and Average Pore Size of the Original and Extracted Samples

	original sample			extracted sample		
sample no.	surface area (m^2/g)	pore volume (cm^3/g)	average pore size (nm)	surface area (m^2/g)	pore volume (cm^3/g)	average pore size (nm)
1	0.2778	0.002352	44.7994	0.6419	0.002996	22.4092
2	0.3182	0.00074	12.7294	0.7426	0.003288	19.283
3	0.3753	0.002172	22.7549	0.5512	0.00244	24.6781
4	1.876	0.006383	16.2154	2.0661	0.007771	15.829
5	0.2046	0.001507	38.0263	0.4115	0.002134	21.0471
6	0.1574	0.001137	41.877	0.2845	0.000951	14.238
7	4.8072	0.017777	15.6004	7.4491	0.019516	13.5472
8	0.885	0.004684	24.9432	1.9776	0.007514	16.4643
9	1.8828	0.006979	16.9216	3.2536	0.009304	12.5391
10	2.314	0.009705	18.4348	2.9163	0.009536	14.1806
11	2.0907	0.011195	21.2397	3.5678	0.011049	12.3313
12	0.72	0.00351	19.1783	1.563	0.006838	17.9075
13	1.1674	0.003532	13.0747	1.5888	0.004543	12.6107
14	4.3079	0.01925	18.9563	9.2133	0.02293	12.7138
15	4.492	0.01721	14.9664	13.5494	0.029241	10.5576
16	4.194	0.02101	18.7548	5.0006	0.018992	18.0335
17	4.9223	0.020926	16.5758	6.5708	0.018178	13.014
18	2.3222	0.009323	14.7163	4.1369	0.010607	12.3878

samples ranges from 0.16 to 4.92 m^2/g, averaging 2.07 m^2/g. After extraction, it varies from 0.28 to 13.55 m^2/g, averaging 3.64 m^2/g. It suggests that shale SSA is increased by solvent extraction. The BJH model shows that the nonextracted sample's pore volume spans from 0.0007 to 0.0210 cm^3/g, with a mean of 0.0089 cm^3/g. The average pore diameter is 21.65 nm, with a range of 12.73 to 44.80 nm. After extraction, the pore volume ranges between 0.0010 and 0.0292 cm^3/g, averaging 0.0104 cm^3/g. The average pore diameter is 15.77 nm, with a range of 10.56 to 24.68 nm. Although the average pore diameter of extracted samples becomes smaller, the pore volume typically increases. It explains why the adsorption capacity of the sample increases after extraction. Moreover, smaller particle sizes generally provide more surface area.[11] In the original state, petroleum occupied part of the tiny pore-throat space, and part of the pores and throats became empty after a long time of solvent extraction. It enlarges the pore volume of the sample and allows smaller pore sizes to be detected.

4. DISCUSSION

4.1. Implications of the Changes in the N_2 Isotherm after Solvent Extraction. Generally, shale reservoirs keep very small pores, mainly nanopores, and a small number of micropores.[13,37,68] N_2 adsorption/desorption isotherms can better characterize the PSD in shale.[25,26] Organic solvent extraction can remove the retained hydrocarbons within shales and restore the real pore system of shale.[19,22,48,67] The SSA and pore size, in addition to pore volume, are important limits on shale adsorption capabilities.[69] The larger surface area and smaller pore diameter enhance petroleum molecules' adsorption and increase the hydrocarbon adsorption potential in the shale systems.[11] Because petroleum occupies the pore surface and pores of shale, it is obvious that larger SSA and pore volume can be released after extraction.

However, the increase or decrease of SSA and pore volume after extraction is mainly controlled by the quantity of hydrocarbons.[18,19] The change in the pore volume and SSA after extraction is minimal when the analyzed sample contains little liquid hydrocarbons. However, when a large amount of petroleum is removed during the extraction process, the increase in pore volume and SSA is even more pronounced.[11,16,18] Nevertheless, the SSA and pore volume of N_2 adsorption increased for most of the samples after petroleum removal, while a few samples still showed a small decrease (Figure 6A,B). The decrease could be due to the constraints of the N_2 adsorption measurement, which is limited to pore measurements in a specific size range (2∼200 nm).[25,70] Some of the recovery spaces after petroleum removal, such as expanded open pore space, maybe outside the measuring range,[11,19,69,71] resulting in a decrease in the pore volume and an increase in SSA. After extraction, except for samples 2 and 3, the average pore diameter of shale decreases significantly (Figure 6C). Solvent extraction causes variations in the average pore size because porosity occurs because of the removal of retained oil.[22] Thus, nanoscale pore throats are released when the petroleum is removed by organic solvents, reducing the shale's average pore size.

4.2. Occurrence State and Space of Shale Oil. *4.2.1. Occurrence Space of Shale Oil.* Pore networks in organic−inorganic components of organic-rich shales play an essential role in hydrocarbon storage.[12,34,72] Furthermore, the large molecular size of shale oil is not present in all of the shale matrix's pores.[15,31] Thus, it is imperative to determine the main occurrence space of shale oil.[19,28,67,73,74] Previous studies have mostly concentrated on the pore structure of shale reservoirs.[20,22,23,28] However, a few studies have focused on the physical state of shale oil,[16,18,32] leaving the relationship between the pore structure and fluid properties unclear. One of the crucial reasons is that the physical state of shale oil is complicated and is difficult to observe and describe directly. For example, traditional FE-SEM or FIB-SEM methods can destroy the sample during specimen preparation or polishing.[61] Therefore, several molecular simulation approaches have been recently proposed to study the occurrence characteristics of hydrocarbons in shale.[75−77] However, because of the complex petroleum molecules and shale composition,[78,79] only simplified petroleum molecules and shale components can be used for modeling, resulting in limited findings. Additionally, NMR technology has been widely applied to study shale pore

https://doi.org/10.1021/acs.energyfuels.2c02222
Energy Fuels 2022, 36, 10920−10933

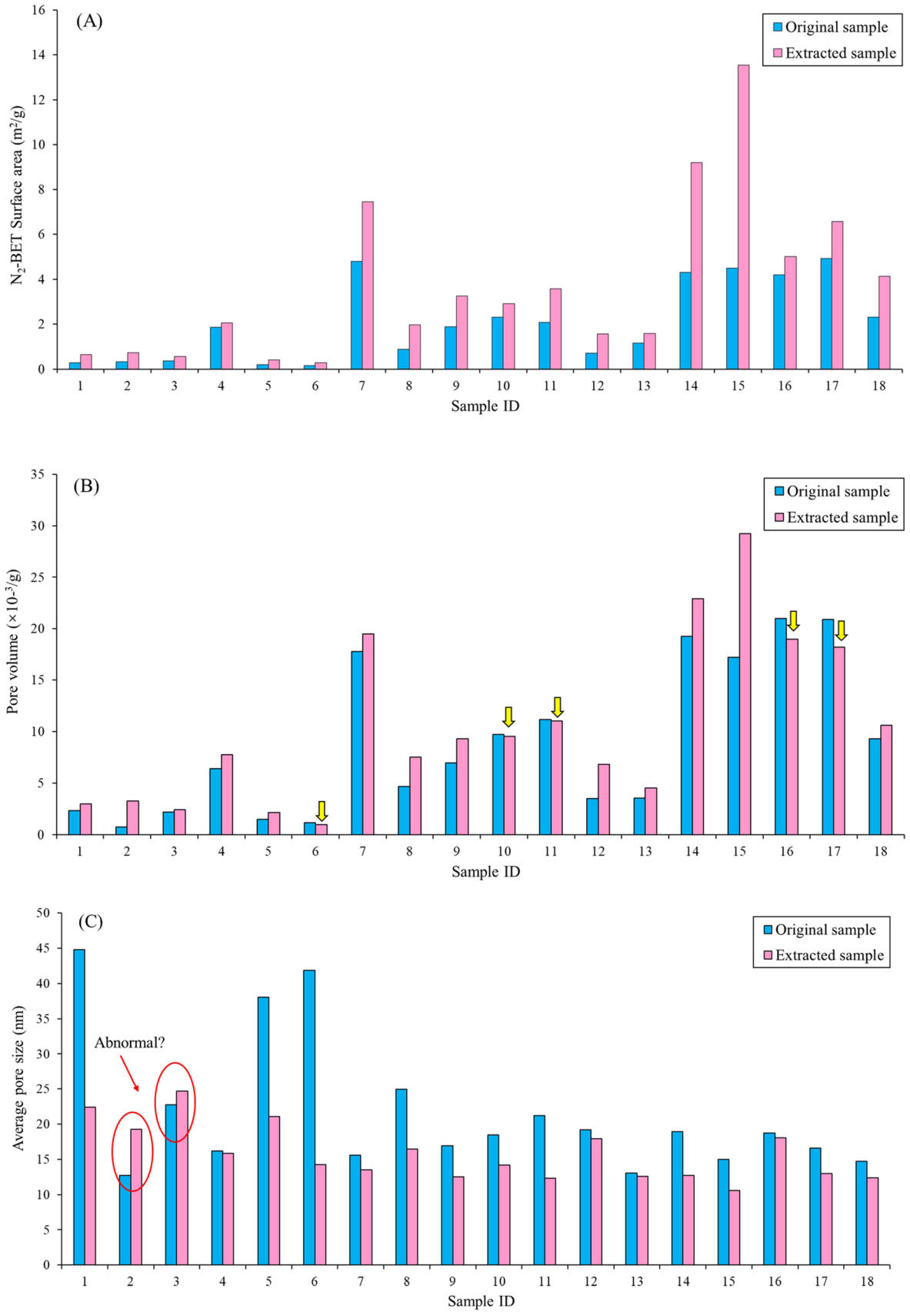

Figure 6. Comparisons of SSA, pore volume, and average pore size before and after extraction. The yellow arrow represents the reduction after extraction.

https://doi.org/10.1021/acs.energyfuels.2c02222
Energy Fuels 2022, 36, 10920−10933

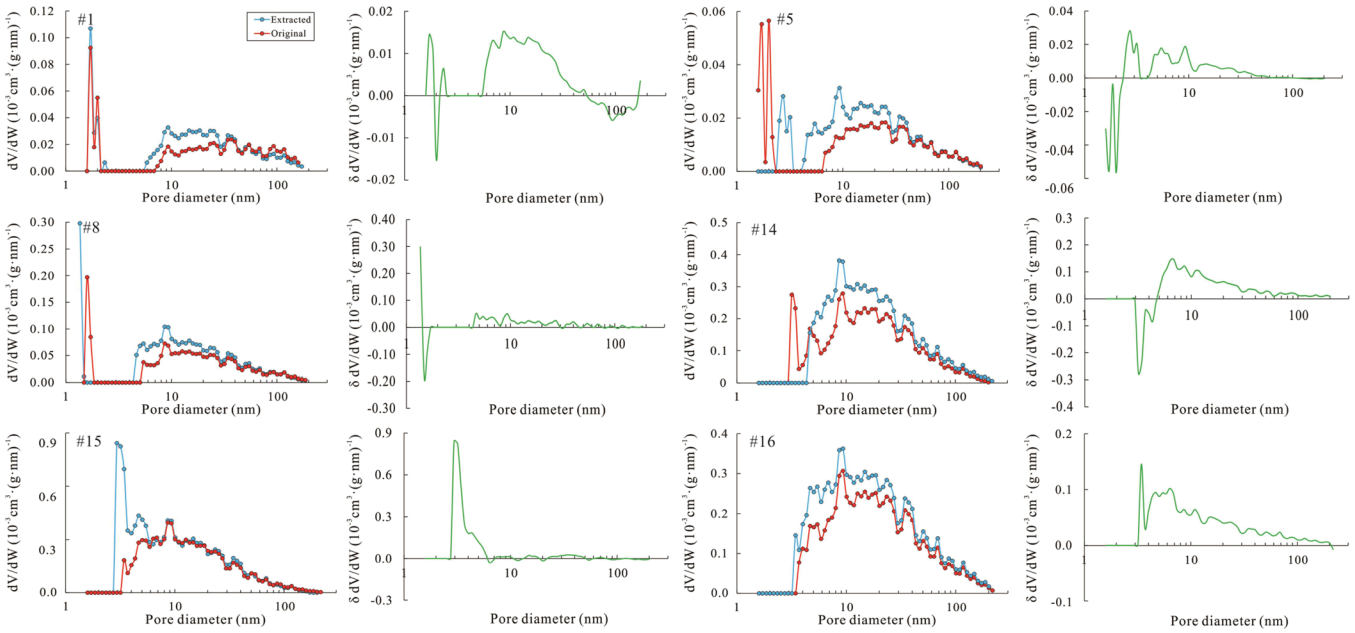

Figure 7. Distribution of average pore diameters and pore volume differences in original and extracted samples.

structure and fluid characteristics.[79−83] Pore distribution characteristics of the shale matrix obtained by 1D-NMR[81,84,85] and the occurrence characteristics of various hydrogen components in shale such as kerogen, asphalt, oil, and water can be obtained by 2D-NMR.[82,83,86] However, hydrogen components in oil-rich shale may overlap and have similar distribution positions.[80] Therefore, it is still debatable how to correctly identify shale oil in various physical states. Additionally, the linkage of oil content with the pore volume and pore size can be used to establish the major pore diameter range of shale oil storage.[31,32]

In this study, the distribution spaces of shale oil are inferred by the pore size change before and after solvent extraction. However, it is difficult to detect when the pore space of the original shale is filled with petroleum, but it can be detected after extraction using organic solvents. Therefore, the occurrence space of shale oil can be determined by comparing the changes in the pore diameter distribution before and after extraction.[23] To begin, we must precisely measure the shale's PSD features. Generally, the PSD can be expressed as the distribution of pore volume with average pore diameter, including incremental pore volume versus diameter (dV), differential pore volume versus diameter (dV/dD), and the log differential pore volume versus diameter ($dV/d\log D$).[3,24,26] The choice of the PSD expression form can affect the understanding of the reservoir pore structure. The results show that the dV/dD is better for describing the pore diameter distribution through the N_2 adsorption method because the curve can reflect more pore information within smaller pore ranges.[70] Additionally, the difference in pore volume distribution ($\delta\, dV/dD$) is utilized to investigate the occurrence space of shale oil in different diameter pores.

Figure 7 shows the dV/dD curves of eight representative samples. The extracted samples have a much greater PSD than the original samples, suggesting that extraction causes the release of petroleum. The two curves are bimodal or multimodal, reflecting the complexity of the shale pore structure.[67,70] Meanwhile, the pore size variation in the micropore curve disorderedly changes before and after extraction, but the PSD's peak remains unaltered. It implies that micropores are not the primary shale oil reservoir space. After extraction, both the mesopore and macropore volumes increase. However, the increase in the mesopore volume is more prominent, indicating that shale oil is largely produced from the mesopore. It seems to be inconsistent with the previous studies, which indicated that the mesopore and the macropore are the main shale oil occurrence space.[34,37,67] It might be due to the larger amount of retained hydrocarbons in the pore space than the pore size range. However, they have not been detected due to evaporation loss during sampling and experiment. The pore volume distribution curve ($\delta\, dV/dD$) reveals that shale oil in the Fengcheng shale mainly occurs in 5−40 nm pore size (Figure 7). The research indicates that shale oil may be recovered from pores as small as 3 nm in diameter. However, it is very difficult to fully obtain shale oil smaller than this pore size. The molecular diameters of n-alkanes, cyclohexane, complex ring structures, and micro-granular bitumen, according to earlier investigations, are 0.48, 0.54, 1−3, and 2.1−2.4 nm, respectively.[87,88] Thus, this part of petroleum is almost impossible to movable during exploitation. The pore distribution of some samples does not change after extraction, indicating a stable pore size, which could be due to the low content of residual oil or the error of the N_2 adsorption experiment.

4.2.2. Occurrence State of Shale Oil. The physical state of shale oil mainly includes free and adsorbed oil.[7,35,37,73] Free oil exists in both inorganic and organic pores,[8,10,37] while adsorbed oil is mainly found on the surface of inorganic minerals and OM.[7,37,89] Although the adsorption capacity of different minerals varies, they have a very low adsorption capacity compared to OM.[89] The mobility of shale oil is significantly reduced because of the strong affinity between adsorbed oil and the pore surface.[15,73,90] Theoretically, free oil is the actual amount of available shale oil, and the free oil in this research designates the movable oil. In previous studies, soluble OM content and pyrolysis S_1 in shale were effective characterization parameters of the oil content.[7,36,48,50,91] However, the adsorbed/free oil was removed simultaneously

https://doi.org/10.1021/acs.energyfuels.2c02222
Energy Fuels 2022, 36, 10920−10933

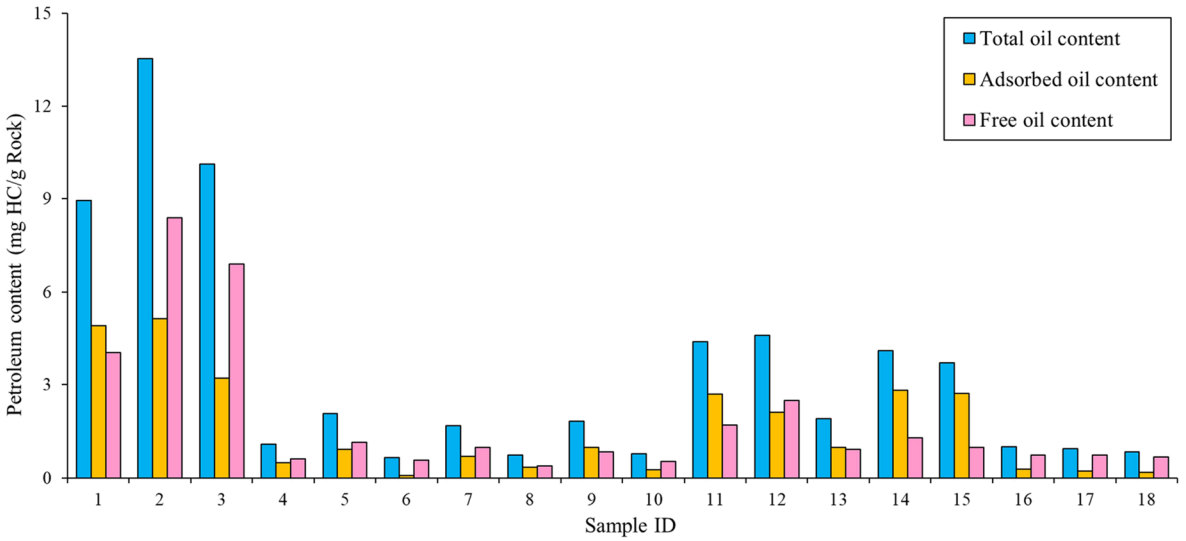

Figure 8. Petroleum content in original shale samples.

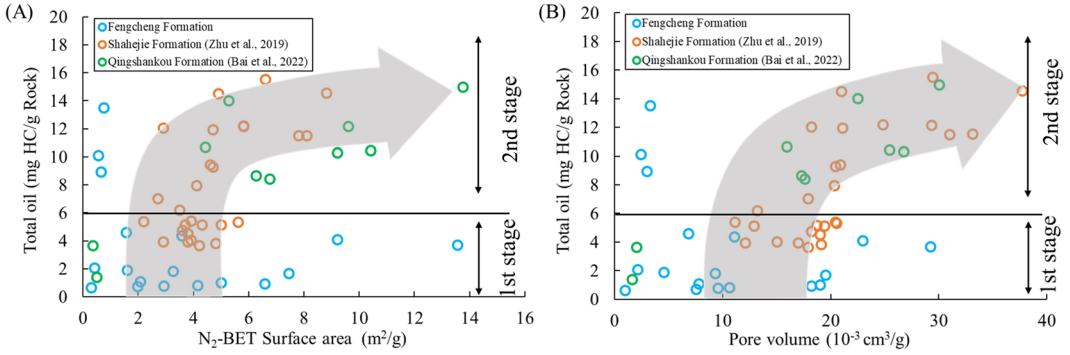

Figure 9. Cross plots of total oil with the SSA and pore volume after extraction.

in the extraction process because the soluble OM could not distinguish the physical state of the oil.[18,92] Therefore, this study does not consider the soluble OM content but directly uses rock pyrolysis parameters to evaluate the shale oil content. Previous scholars also characterized free oil in shale through pyrolysis methods.[1,7,10,46] Jarvie[7,44] proposed a new method to eliminate the influence of the carryover effect. According to that method, the total oil in shale could be expressed as total oil yield (TOY) = $(S_1 - S_{1\text{Extracted}}) + (S_2 - S_{2\text{Extracted}})$, and the adsorbed oil yield can be expressed as AOY = $S_2 - S_{2\text{Extracted}} - S_{1\text{Extracted}}$. Therefore, the movable oil yield (MOY) can be quantitatively characterized by TOY-AOY.

Figure 8 shows the fluctuation of TOY, MOY, and AOY in the Fengcheng shale samples before and after extraction. MOY and TOY have significant positive association, indicating that the overall amount of MOY in the shale oil-rich area is quite large. The TOY of the Fengcheng shale ranges from 0.65 mg HC/g Rock to 13.52 mg HC/g Rock, averaging 3.49 mg HC/g Rock. The AOY varies from 0.08 mg HC/g Rock to 5.13 mg HC/g Rock, averaging 1.61 mg HC/g Rock. MOY ranges from 0.57 to 8.39 mg HC/g Rock, with a typical value of 1.88 mg HC/g. Through pyrolysis methods, Li et al.[50] calculated the shale resource amount of Shahejie Formation in Dongying Sag (Bohai Bay Basin) and obtained the proportion of free oil that varies between 44.70 and 55.80%. Guo et al.[49] used similar methods to evaluate shale oil in Chang 7 member of Ordos Basin and obtained that the ratio of MOY to TOY is 37.00%. In this study, the average proportion of free oil in the Fengcheng shale of the Junggar Basin is high (57.17%), indicating that shale oil has great exploitation potential.

The correlations of total oil with the N_2-BET SSA and pore volume after solvent extraction (Figure 9A,B) appear to have two stages. It is simple to comprehend when considering it in terms of the generation process of hydrocarbons. The evolution of hydrocarbon from organic-rich shale starts with the conversion of kerogen to hydrocarbons.[87] At the early stage of hydrocarbon generation, the molecular structural differences between hydrocarbons and kerogen are minor, and their adsorption affinity is strong. In this case, petroleum is mainly adsorbed on the surface of kerogen and the microfracture surface of kerogen.[15,32] Furthermore, the inorganic pores of clay minerals with a high SSA can still be the shale oil adsorption sites.[89,93] As hydrocarbon production increases, the amount of petroleum produced may exceed the maximal adsorption and storage capacity of organic-matter pores. As a result, shale oil begins to migrate into smaller inorganic pores and microfractures.[94] Moreover, it gradually covers inorganic minerals' surface and pore space until it saturates the shale pores.[18] At this stage, both free and adsorbed hydrocarbons are present in shale systems. Based on the above hypothesis, the free oil occurs when the generated petroleum is sufficient to meet kerogen and inorganic minerals adsorption, and it continuously enriches and saturates the shale pores. As a

https://doi.org/10.1021/acs.energyfuels.2c02222
Energy Fuels 2022, 36, 10920−10933

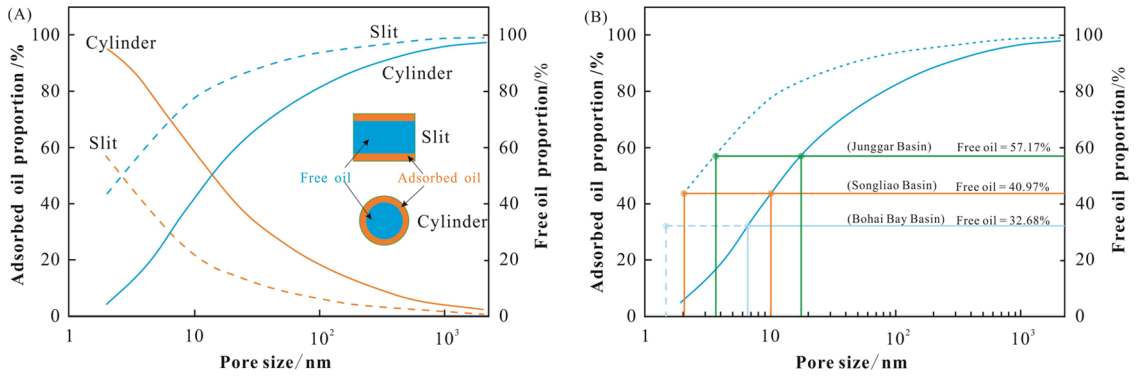

Figure 10. (A) Variation in volume fraction of adsorbed oil and free oil with pore size in different shape pores (modified after Dang et al.[74]), (B) thresholds of pore size limiting the petroleum mobility of shale in different basins (the intersection points on the dotted/solid line represent the limit when slit/cylindrical pores are fully developed in shale).

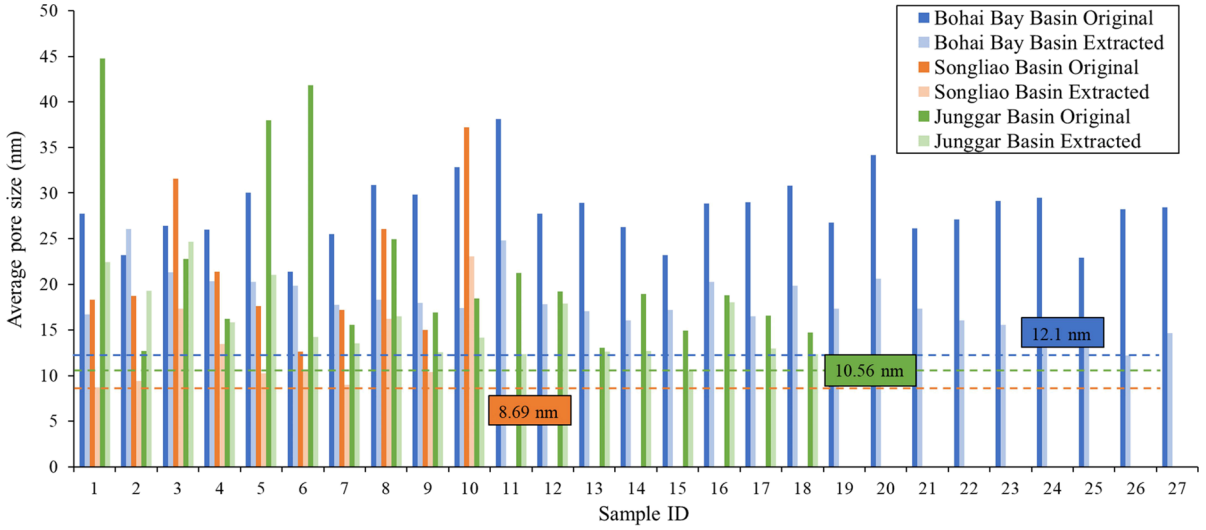

Figure 11. Thresholds of the pore diameter limit the movable oil in the shale in different basins.

result, free oil content increases in tandem with the SSA and pore volume.

4.2.3. Thresholds of Movable Oil. The threshold of petroleum mobility is the key to unconventional resource exploration. Compared to adsorbed oil, free oil contributes more to the overall shale oil production.[15,90] Some researchers have long struggled with determining the lowest limit of the pore diameter of movable oil. Through physical simulation experiments, Zou et al.[34] proposed that oil in pores with pore sizes above 20 nm can flow freely. Wang et al.[32] determined that the threshold pore size of movable oil is about 30 nm through the relationship between free oil obtained from multistep pyrolysis and the pore throat size. Zhu et al.[18] and Bai et al.[16] established the movable oil thresholds by changing the pore size before and after extraction to be 12.1 and 10 nm, respectively. These disparate conclusions reveal a divergence of views on the scientific issue.

In this study, both free and adsorbed oil were washed away during the extraction process with the organic solvent.[18,44,92] Therefore, the relationship between the distribution of movable oil (free oil) and pore distribution cannot be determined from the difference in pores before and after extraction. Hence, this research analyzes the experimental data of shale in three different lacustrine basins (Junggar, Bohai Bay, and Songliao Basins) to determine the minimum oil content when movable oil occurs and the threshold of pore size corresponding to movable oil (Figure 9A,B). However, the significant inflection point arises when the total oil yield in the shale reaches about 6 mg HC/g Rock, which represents the transition between the two stages of the oil charging process. When the petroleum content of shale oil exceeds this threshold, it can exist in huge amounts as free oil, resulting in the phenomenon of oil being moveable. In addition to the percentage of retained hydrocarbon, the pore size threshold of movable oil is intimately related to the pore properties of shale. The reason is that the physical state of shale oil has a strong pore dependence.[74,75] Different pores will produce different adsorption effects, for example, cylindrical pores compared with slit pores will increase the proportion of oil adsorption.[74,75] According to the theory of adsorbed oil film thickness, the ratio of adsorbed/free oil in cylindrical pores and parallel plate pores under different pore sizes was calculated using the volume calculation formula[74,75] (Figure 10A). Moreover, it can be used to evaluate the pore size range of movable shale oil in different basins (Figure 10B). Based on the proportion of free/adsorbed oil in shales from different basins, the threshold of movable oil in the two pore types can be inferred. According to the results of theoretical calculation, the pore size threshold of movable oil in the Shahejie Formation (Bohai Bay Basin) is about 7 nm, while in the

https://doi.org/10.1021/acs.energyfuels.2c02222
Energy Fuels 2022, 36, 10920−10933

Qingshankou Formation (Songliao Basin) is between 2 and 10 nm. In contrast, the pore size threshold of the P_1f in Junggar Basin is about 3.5−19 nm. The Fengcheng shale is dominated by slit pores, which provides good spatial foundation for the favorable occurrence of shale oil (i.e., high free oil/adsorbed oil ratio). The lower limit of the petroleum pore diameter obtained via solvent extraction is shown in Figure 11, which is much higher than the theoretically calculated pore size of movable oil. The following are possible explanations. First, the data of N_2 adsorption before and after extraction calculate the change in the average pore size, but the threshold limit of movable oil may be lower for a specific pore. Second, the solvent extraction process contains both free oil and some adsorbed oil. Third, the oil-rock interaction in shale is substantially more complicated, making it impossible to accurately estimate adsorbed oil film thickness. Despite these disparities, we prefer to use the upper limit of the movable oil range as the threshold of movable oil. When the pore diameter exceeds this threshold, the shale pores are mostly occupied by movable oil, which can be effectively utilized in the exploitation process.

5. CONCLUSIONS

(1) Based on the analysis of shale oil content in various occurrence states, evaluation parameters are obtained by two-step rock pyrolysis to calculate the resource potential of different types of shale oil. The total oil content of the Fengcheng shale is 3.49 mg HC/g Rock, with free oil accounting for 57.17%. It indicates the Fengcheng Formation's significant shale oil exploitation prospects.

(2) The distribution features of retained hydrocarbons are systematically evaluated. According to the statistics of oil content and pore volume of shale with various pore sizes in the Fengcheng shale, shale oil is primarily distributed in mesopore pores with diameters of 5−40 nm. The threshold limit of the pore diameter for the movable oil in the shale is between 3.5 and 19 nm.

(3) Statistical analysis of data from different basins shows that petroleum mobility occurs when the total oil yield in shale reaches 6 mg HC/g Rock. The lower limit of the pore size of movable oil is different in different basins, which is related to the pore structure of shale. The threshold limit of the pore diameter for movable oil is low when parallel plate pores dominate the shale, while it is higher when cylindrical pores dominate the shale.

AUTHOR INFORMATION

Corresponding Authors

Chenglin Liu − *State Key Laboratory of Petroleum Resources and Prospecting and College of Geosciences, China University of Petroleum, Beijing 102249, China*; Email: liucl@cup.edu.cn

Fujie Jiang − *State Key Laboratory of Petroleum Resources and Prospecting and College of Geosciences, China University of Petroleum, Beijing 102249, China*; Email: jiangfj@cup.edu.cn

Authors

Yuping Wu − *State Key Laboratory of Petroleum Resources and Prospecting and College of Geosciences, China University of Petroleum, Beijing 102249, China; Department of Chemical and Petroleum Engineering, University of Calgary, Calgary T2N 1N4, Canada*; orcid.org/0000-0002-6701-5886

Tao Hu − *State Key Laboratory of Petroleum Resources and Prospecting and College of Geosciences, China University of Petroleum, Beijing 102249, China*

Rizwan Sarwar Awan − *School of Resources and Environmental Engineering, Hefei University of Technology, Hefei 230009, China*

Zhangxin Chen − *Department of Chemical and Petroleum Engineering, University of Calgary, Calgary T2N 1N4, Canada*; orcid.org/0000-0002-9107-1925

Jiahao Lv − *State Key Laboratory of Petroleum Resources and Prospecting and College of Geosciences, China University of Petroleum, Beijing 102249, China*

Chenxi Zhang − *State Key Laboratory of Petroleum Resources and Prospecting and College of Geosciences, China University of Petroleum, Beijing 102249, China*

Meiling Hu − *State Key Laboratory of Petroleum Resources and Prospecting and College of Geosciences, China University of Petroleum, Beijing 102249, China*

Renda Huang − *State Key Laboratory of Petroleum Resources and Prospecting and College of Geosciences, China University of Petroleum, Beijing 102249, China*

Guanyun Wu − *State Key Laboratory of Petroleum Resources and Prospecting and College of Geosciences, China University of Petroleum, Beijing 102249, China*

Complete contact information is available at: https://pubs.acs.org/10.1021/acs.energyfuels.2c02222

Notes

The authors declare no competing financial interest.

ACKNOWLEDGMENTS

Financial support from the Strategic Cooperation Technology Projects of CNPC and CUPB (ZLZX2020-01-05), the National Natural Science Foundations of China (41872127, 41872128), the National Key R&D Program of China (2021YFA0719000), the Science Foundation of China University of Petroleum (Beijing) (2462019BJRC005), the Young Talents Support Project of Beijing Science and Technology Association (ZX20210075), as well as the China Scholarship Council (CSC).

REFERENCES

(1) Li, M.; Chen, Z.; Ma, X.; Cao, T.; Qian, M.; Jiang, Q.; Tao, G.; Li, Z.; Song, G. Shale oil resource potential and oil mobility characteristics of the Eocene-Oligocene Shahejie Formation, Jiyang Super-Depression, Bohai Bay Basin of China. *Int. J. Coal Geol.* **2019**, *204*, 130−143.

(2) Jin, Z.; Liang, X.; Bai, Z. Exploration breakthrough and its significance of Gulong lacustrine shale oil in the Songliao Basin, Northeastern China. *Energy Geosci.* **2022**, *3*, 120−125.

(3) Li, Y.; Wang, Z.; Pan, Z.; Niu, X.; Yu, Y.; Meng, S. Pore structure and its fractal dimensions of transitional shale: A cross-section from east margin of the Ordos Basin, China. *Fuel* **2019**, *241*, 417−431.

(4) Li, Y.; Pan, S.; Ning, S.; Shao, L.; Jing, Z.; Wang, Z. Coal measure metallogeny: Metallogenic system and implication for resource and environment. *Sci. China Earth Sci.* **2022**, *65*, 1211−1228.

(5) Hu, T.; Pang, X.; Xu, T.; Li, C.; Jiang, S.; Wang, Q.; Chen, Y.; Zhang, H.; Huang, C.; Gong, S.; Gao, Z. Identifying the key source rocks in heterogeneous saline lacustrine shales: Paleogene shales in the Dongpu depression, Bohai Bay Basin, eastern China. *AAPG Bull.* **2022**, *106*, 1325−1356.

(6) Zhao, W.; Zhang, B.; Wang, X.; Wu, S.; Zhang, S.; Liu, W.; Wang, K.; Zhao, X. Differences in source kitchens for lacustrine in-source and out-of-source hydrocarbon accumulations. *Pet. Explor. Dev.* **2021**, *48*, 541−554.
(7) Jarvie, D. M. Shale Resource Systems for Oil and Gas Part 2: Shale-oil Resource Systems. In *Shale Reservoirs—Giant Resources for the 21st Century: AAPG Memoir*; American Association of Petroleum Geologists, 2012; Vol. *97*, pp 89−119.
(8) Sang, Q.; Zhang, S.; Li, Y.; Dong, M.; Bryant, S. Determination of organic and inorganic hydrocarbon saturations and effective porosities in shale using vacuum-imbibition method. *Int. J. Coal Geol.* **2018**, *200*, 123−134.
(9) Bustin, A. M. M.; Bustin, R. M. Importance of rock properties on the producibility of gas shales. *Int. J. Coal Geol.* **2012**, *103*, 132−147.
(10) Loucks, R. G.; Reed, R. M.; Ruppel, S. C.; Jarvie, D. M. Morphology, Genesis, and Distribution of Nanometer-Scale Pores in Siliceous Mudstones of the Mississippian Barnett Shale. *J. Sediment. Res.* **2009**, *79*, 848−861.
(11) Lin, W.; Maria, M.; Arndt, S.; Chen, Y. Influence of Soxhlet-extractable bitumen and oil on porosity in thermally maturing organic-rich shales. *Int. J. Coal Geol.* **2014**, *132*, 38−50.
(12) Ko, L. T.; Loucks, R. G.; Ruppel, S. C.; Zhang, T.; Peng, S. Origin and characterization of Eagle Ford pore networks in the south Texas Upper Cretaceous shelf. *AAPG Bull.* **2017**, *101*, 387−418.
(13) Loucks, R. G.; Reed, R. M.; Ruppel, S. C.; Hammes, U. Spectrum of pore types and networks in mudrocks and a descriptive classification for matrix-related mudrock pores. *AAPG Bull.* **2012**, *96*, 1071−1098.
(14) Ko, L. T.; Loucks, R. G.; Zhang, T.; Ruppel, S. C.; Shao, D. Pore and pore network evolution of Upper Cretaceous Boquillas (Eagle Ford−equivalent) mudrocks: Results from gold tube pyrolysis experiments. *AAPG Bull.* **2016**, *100*, 1693−1722.
(15) Xu, Y.; Lun, Z.; Pan, Z.; Wang, H.; Zhou, X.; Zhao, C.; Zhang, D. Occurrence space and state of shale oil: A review. *J. Pet. Sci. Eng.* **2022**, *211*, No. 110183.
(16) Bai, L.-H.; Liu, B.; Du, Y.-J.; Wang, B.-Y.; Tian, S.-S.; Wang, L.; Xue, Z.-Q. Distribution characteristics and oil mobility thresholds in lacustrine shale reservoir: Insights from N2 adsorption experiments on samples prior to and following hydrocarbon extraction. *Pet. Sci.* **2022**, *19*, 486−497.
(17) Gao, Z.; Xuan, Q.; Hu, Q.; Jiang, Z.; Liu, X. Pore structure evolution characteristics of continental shale in China as indicated from thermal simulation experiments. *AAPG Bull.* **2021**, *105*, 2159−2180.
(18) Zhu, X.; Cai, J.; Liu, Q.; Li, Z.; Zhang, X. Thresholds of petroleum content and pore diameter for petroleum mobility in shale. *AAPG Bull.* **2019**, *103*, 605−617.
(19) Lei, Y.; Luo, X.; Wang, X.; Cheng, M.; Zhang, L.; Cai, Z.; Zhang, L.; Jiang, C.; Zhao, Q. P.; Yin, J. Effects of extractable organic matter from mature lacustrine shale on the pore structure and their implications. *AAPG Bull.* **2022**, *106*, 1239−1264.
(20) Zargari, S.; Canter, K. L.; Prasad, M. Porosity evolution in oil-prone source rocks. *Fuel* **2015**, *153*, 110−117.
(21) DiStefano, V. H.; McFarlane, J.; Anovitz, L. M.; Stack, A. G.; Gordon, A. D.; Littrell, K. C.; Chipera, S. J.; Hunt, R. D.; Lewis, S. A.; Hale, R. E.; Perfect, E. Extraction of organic compounds from representative shales and the effect on porosity. *J. Nat. Gas Sci. Eng.* **2016**, *35*, 646−660.
(22) Li, J.; Zhou, S.; Li, Y.; Ma, Y.; Yang, Y.; Li, C. Effect of organic matter on pore structure of mature lacustrine organic-rich shale: A case study of the Triassic Yanchang shale, Ordos Basin, China. *Fuel* **2016**, *185*, 421−431.
(23) Liu, C.; Xu, X.; Liu, K.; Bai, J.; Liu, W.; Chen, S. Pore-scale oil distribution in shales of the Qingshankou formation in the Changling Sag, Songliao Basin, NE China. *Mar. Pet. Geol.* **2020**, *120*, No. 104553.
(24) Ji, W. M.; Song, Y.; Rui, Z. H.; Meng, M. M.; Huang, H. X. Pore characterization of isolated organic matter from high matured gas shale reservoir. *Int. J. Coal Geol.* **2017**, *174*, 31−40.
(25) Clarkson, C. R.; Solano, N.; Bustin, R. M.; Bustin, A. M. M.; Chalmers, G. R. L.; He, L.; Melnichenko, Y. B.; Radliński, A. P.; Blach, T. P. Pore structure characterization of North American shale gas reservoirs using USANS/SANS, gas adsorption, and mercury intrusion. *Fuel* **2013**, *103*, 606−616.
(26) Labani, M. M.; Rezaee, R.; Saeedi, A.; Hinai, A. A. Evaluation of pore size spectrum of gas shale reservoirs using low pressure nitrogen adsorption, gas expansion and mercury porosimetry: A case study from the Perth and Canning Basins, Western Australia. *J. Pet. Sci. Eng.* **2013**, *112*, 7−16.
(27) Chalmers, G. R.; Bustin, R. M.; Power, I. M. Characterization of gas shale pore systems by porosimetry, pycnometry, surface area, and field emission scanning electron microscopy/transmission electron microscopy image analyses: Examples from the Barnett, Woodford, Haynesville, Marcellus, and Doig units. *AAPG Bull.* **2012**, *96*, 1099−1119.
(28) Liu, D.; Su, J.; Gu, Z.; Qi, Y.; Yang, F.; Tian, T.; Ye, F.; Zhan, S. Geochemical Properties and Pore Structure Control on Oil Extraction of Shale. *Lithosphere* **2021**, *2021*, No. 6646791.
(29) Li, Y.; Chen, J.; Elsworth, D.; Pan, Z.; Ma, X. Nanoscale mechanical property variations concerning mineral composition and contact of marine shale. *Geosci. Front.* **2022**, *13*, No. 101405.
(30) Li, Y.; Yang, J.; Pan, Z.; Tong, W. Nanoscale pore structure and mechanical property analysis of coal: An insight combining AFM and SEM images. *Fuel* **2020**, *260*, No. 116352.
(31) Wang, M.; Yang, J.; Wang, Z.; Lu, S. Nanometer-Scale Pore Characteristics of Lacustrine Shale, Songliao Basin, NE China. *PLoS One* **2015**, *10*, No. e0135252.
(32) Wang, M.; Ma, R.; Li, J.; Lu, S.; Li, Z. Occurrence mechanism of lacustrine shale oil in the Paleogene Shahejie Formation of Jiyang Depression, Bohai Bay Basin, China. *Pet. Explor. Dev.* **2019**, *46*, 833−846.
(33) Zou, C.; Zhu, R.; Wu, S.; Yang, Z.; Tao, S.; Yuan, X.; Hou, L.; Yang, H.; Xu, C.; Li, D.; Bai, B.; Wang, L. Types, characteristics, genesis and prospects of conventional and unconventional hydrocarbon accumulations: taking tight oil and tight gas in China as an instance. *Acta Pet. Sin* **2012**, *33*, 173−187.
(34) Zou, C.; Jin, X.; Zhu, R.; Gong, G.; Sun, L.; Dai, J.; Meng, D.; Wang, X.; Li, J.; Wu, S.; Jiang, L. Do Shale Pore Throats Have a Threshold Diameter for Oil Storage? *Scientific Reports* **2015**, *5* (1), 1−6.
(35) Han, Y.; Horsfield, B.; Wirth, R.; Mahlstedt, N.; Bernard, S. Oil retention and porosity evolution in organic rich shales. *AAPG Bull.* **2017**, *101*, 807−827.
(36) Hu, T.; Pang, X. Q.; Jiang, F. J.; Wang, Q. F.; Liu, X. H.; Wang, Z.; Jiang, S.; Wu, G. Y.; Li, C. J.; Xu, T. W.; Li, M. W.; Yu, J. W.; Zhang, C. X. Movable oil content evaluation of lacustrine organic-rich shales: Methods and a novel quantitative evaluation model. *Earth-Sci. Rev.* **2021**, *214*, No. 103545.
(37) Zou, C.; Yang, Z.; Cui, J.; Zhu, R.; Hou, L.; Tao, S.; Yuan, X.; Wu, S.; Lin, S.; Wang, L. Formation mechanism, geological characteristics and development strategy of nonmarine shale oil in China. *Pet. Explor. Dev.* **2013**, *40*, 15−27.
(38) Zhang, H.; Huang, H.; Li, Z.; Liu, M. Oil physical status in lacustrine shale reservoirs − A case study on Eocene Shahejie Formation shales, Dongying Depression, East China. *Fuel* **2019**, *257*, No. 116027.
(39) Zhang, H.; Huang, H.; Li, Z.; Liu, M. Comparative study between sequential solvent-extraction and multiple isothermal stages pyrolysis: A case study on Eocene Shahejie Formation shales, Dongying Depression, East China. *Fuel* **2020**, *263*, No. 116591.
(40) Chen, Z.; Li, M.; Ma, X.; Cao, T.; Liu, X.; Li, Z.; Jiang, Q.; Wu, S. Generation kinetics based method for correcting effects of migrated oil on Rock-Eval data − An example from the Eocene Qianjiang Formation, Jianghan Basin, China. *Int. J. Coal Geol.* **2018**, *195*, 84−101.
(41) Romero-Sarmiento, M.-F. A quick analytical approach to estimate both free versus sorbed hydrocarbon contents in liquid-rich source rocks. *AAPG Bull.* **2019**, *103*, 2031−2043.

https://doi.org/10.1021/acs.energyfuels.2c02222
Energy Fuels 2022, 36, 10920−10933

(42) Carvajal-Ortiz, H.; Gentzis, T. Critical considerations when assessing hydrocarbon plays using Rock-Eval pyrolysis and organic petrology data: Data quality revisited. *Int. J. Coal Geol.* **2015**, *152*, 113−122.
(43) Gorynski, K. E.; Tobey, M. H.; Enriquez, D. A.; Smagala, T. M.; Dreger, J. L.; Newhart, R. E. Quantification and characterization of hydrocarbon-filled porosity in oil-rich shales using integrated thermal extraction, pyrolysis, and solvent extraction. *AAPG Bull.* **2019**, *103*, 723−744.
(44) Jarvie, D. M. *Petroleum Systems in the Permian Basin: Targeting Optimum Oil Production*; Huston Geological Society: Houston, Texas, 2018.
(45) Zink, K. G.; Scheeder, G.; Stueck, H. L.; Biermann, S.; Blumenberg, M. Total shale oil inventory from an extended Rock-Eval approach on non-extracted and extracted source rocks from Germany. *Int. J. Coal Geol.* **2016**, *163*, 186−194.
(46) Abrams, M. A.; Gong, C.; Garnier, C.; Sephton, M. A. A new thermal extraction protocol to evaluate liquid rich unconventional oil in place and in-situ fluid chemistry. *Mar. Pet. Geol.* **2017**, *88*, 659−675.
(47) Li, M.; Chen, Z.; Qian, M.; Ma, X.; Jiang, Q.; Li, Z.; Tao, G.; Wu, S. What are in pyrolysis S1 peak and what are missed? Petroleum compositional characteristics revealed from programed pyrolysis and implications for shale oil mobility and resource potential. *Int. J. Coal Geol.* **2020**, *217*, 104707.
(48) Han, Y.; Mahlstedt, N.; Horsfield, B. The Barnett Shale: Compositional fractionation associated with intraformational petroleum migration, retention, and expulsion. *AAPG Bull.* **2015**, *99*, 2173−2202.
(49) Guo, Q.; Chen, X.; Liuzhuang, X.; Yang, Z.; Zheng, M.; Chen, N.; Mi, J. Evaluation method for resource potential of shale oil in the Triassic Yanchang Formation of the Ordos Basin, China. *Energy Explor. Exploit.* **2020**, *38*, 841−866.
(50) Li, M.; Chen, Z.; Ma, X.; Cao, T.; Li, Z.; Jiang, Q. A numerical method for calculating total oil yield using a single routine Rock-Eval program: A case study of the Eocene Shahejie Formation in Dongying Depression, Bohai Bay Basin China. *Int. J. Coal Geol.* **2018**, *191*, 49−65.
(51) Ziegs, V.; Horsfield, B.; Skeie, J. E.; Rinna, J. Petroleum retention in the Mandal Formation, Central Graben, Norway. *Mar. Pet. Geol.* **2017**, *83*, 195−214.
(52) Cao, J.; Xia, L.; Wang, T.; Zhi, D.; Tang, Y.; Li, W. An alkaline lake in the Late Paleozoic Ice Age (LPIA): A review and new insights into paleoenvironment and petroleum geology. *Earth-Sci. Rev.* **2020**, *202*, No. 103091.
(53) Guo, P.; Wen, H.; Gibert, L.; Jin, J.; Jiang, Y.; Wang, G. Controlling factors of high-quality hydrocarbon source rocks developed in lacustrine shallow-water zone of the Junggar Basin, northwestern China. *AAPG Bull.* **2021**, *105*, 2063−2092.
(54) Yu, K.; Cao, Y.; Qiu, L.; Sun, P.; Jia, X.; Wan, M. Geochemical characteristics and origin of sodium carbonates in a closed alkaline basin: The Lower Permian Fengcheng Formation in the Mahu Sag, northwestern Junggar Basin, China. *Palaeogeogr., Palaeoclimatol., Palaeoecol.* **2018**, *511*, 506−531.
(55) Xia, L.; Cao, J.; Stüeken, E. E.; Zhi, D.; Wang, T.; Li, W. Unsynchronized evolution of salinity and pH of a Permian alkaline lake influenced by hydrothermal fluids: A multi-proxy geochemical study. *Chem. Geol.* **2020**, *541*, No. 119581.
(56) Wu, Y.; Liu, C.; Jiang, F.; Hu, T.; Lv, J.; Zhang, C.; Guo, X.; Huang, L.; Hu, M.; Huang, R.; Awan, R. S.; Zhao, Y. Geological characteristics and shale oil potential of alkaline lacustrine source rock in Fengcheng Formation of the Mahu Sag, Junggar Basin, Western China. *J. Pet. Sci. Eng.* **2022**, *216*, No. 110823.
(57) Xia, L.; Cao, J.; Lee, C.; Stueken, E. E.; Zhi, D.; Love, G. D. A new constraint on the antiquity of ancient haloalkaliphilic green algae that flourished in a ca. 300 Ma Paleozoic lake. *Geobiology* **2021**, *19*, 147−161.
(58) Brunauer, S.; Emmet, P. H.; Teller, E. Adsorption of gases in multimolecular layers. *J. Am. Chem. Soc.* **1938**, *60*, 309−319.
(59) Barrett, E. P.; Joyner, L. G.; Halenda, P. P. The determination of pore volume and area distributions in porous substances. I. Computations from nitrogen isotherms. *J. Am. Chem. Soc.* **1951**, *73*, 373−380.
(60) Do, D. D.; Do, D. H. Pore Characterization of Carbonaceous Materials by DFT and GCMC Simulations: A Review. *Adsorpt. Sci. Technol.* **2003**, *21*, 389−423.
(61) Curtis, M. E.; Sondergeld, C. H.; Ambrose, R. J.; Rai, C. S. Microstructural investigation of gas shales in two and three dimensions using nanometer-scale resolution imaging. *AAPG Bull.* **2012**, *96*, 665−677.
(62) Curtis, M. E.; Cardott, B. J.; Sondergeld, C. H.; Rai, C. S. Development of organic porosity in the Woodford Shale with increasing thermal maturity. *Int. J. Coal Geol.* **2012**, *103*, 26−31.
(63) Romero-Sarmiento, M.-F.; Pillot, D.; Letort, G.; Lamoureux-Var, V.; Beaumont, V.; Huc, A.-Y.; Garcia, B. New Rock-Eval Method for Characterization of Unconventional Shale Resource Systems. *Oil Gas Sci. Technol.* **2015**, *71*, 37.
(64) Collins, D. R.; Lapierre, S. *Integrating Solvent Extraction With Standard Pyrolysis to Better Quantify Thermal Maturity and Hydrocarbon Content in the Oil Window*; Unconventional Resources Technology Conference, 2014; 2014.
(65) Chen, K.; Zhang, T.; Chen, X.; He, Y.; Liang, X. Model construction of micro-pores in shale: A case study of Silurian Longmaxi Formation shale in Dianqianbei area, SW China. *Pet. Explor. Dev.* **2018**, *45*, 412−421.
(66) Sing, K.; Everett, D. H.; Haul, R.; Moscou, L.; Pierotti, R. A.; Rouquerol, J.; Siemieniewska, T. Reporting physisorption data for gas/solid systems with Special Reference to the Determination of Surface Area and Porosity. *Pure Appl. Chem.* **1985**, *57*, 603−619.
(67) Su, S.; Jiang, Z.; Xuanlong, S.; Zhang, C.; Zou, Q.; Li, Z.; Zhu, R. The effects of shale pore structure and mineral components on shale oil accumulation in the Zhanhua Sag, Jiyang Depression, Bohai Bay Basin, China. *J. Pet. Sci. Eng.* **2018**, *165*, 365−374.
(68) Huang, H.; Li, R.; Jiang, Z.; Li, J.; Chen, L. Investigation of variation in shale gas adsorption capacity with burial depth: Insights from the adsorption potential theory. *J. Nat. Gas Sci. Eng.* **2020**, *73*, 104344.
(69) Furmann, A.; Mastalerz, M.; Brassell, S. C.; Schimmelmann, A.; Picardal, F. Extractability of biomarkers from high- and low-vitrinite coals and its effect on the porosity of coal. *Int. J. Coal Geol.* **2013**, *107*, 141−151.
(70) Liu, K.; Ostadhassan, M. The impact of pore size distribution data presentation format on pore structure interpretation of shales. *Adv. Geo-Energy Res.* **2019**, *3*, 187−197.
(71) Wang, Y.; Liu, L.; Cheng, H. Pore structure of Triassic Yanchang mudstone, Ordos Basin: Insights into the impact of solvent extraction on porosity in lacustrine mudstone within the oil window. *J. Pet. Sci. Eng.* **2020**, *195*, No. 107944.
(72) Huang, H.; Li, R.; Xiong, F.; Hu, H.; Sun, W.; Jiang, Z.; Chen, L.; Wu, L. A method to probe the pore-throat structure of tight reservoirs based on low-field NMR: Insights from a cylindrical pore model. *Mar. Pet. Geol.* **2020**, *117*, No. 104344.
(73) Zhu, C.; Guo, W.; Li, Y.; Gong, H.; Sheng, J. J.; Dong, M. Effect of occurrence states of fluid and pore structures on shale oil movability. *Fuel* **2021**, *288*, No. 119847.
(74) Dang, W.; Zhang, J.; Nie, H.; Wang, F.; Tang, X.; Jiang, S.; Wei, X.; Liu, Q.; Li, P.; Li, F.; Sun, J. Microscopic occurrence characteristics of shale oil and their main controlling factors:a case study of the 3rd submember continental shale of Member 7 of Yanchang Formation in Yan'an area, Ordos Basin. *Acta Pet. Sin.* **2022**, *43*, 507−523.
(75) Wang, S.; Feng, Q.; Javadpour, F.; Xia, T.; Li, Z. Oil adsorption in shale nanopores and its effect on recoverable oil-in-place. *Int. J. Coal Geol.* **2015**, *147−148*, 9−24.
(76) Zhang, Y.; Guo, W. Molecular insight into the tight oil movability in nano-pore throat systems. *Fuel* **2021**, *293*, No. 120428.

https://doi.org/10.1021/acs.energyfuels.2c02222
Energy Fuels 2022, 36, 10920−10933

(77) Zhang, W.; Feng, Q.; Wang, S.; Xing, X. Oil diffusion in shale nanopores: Insight of molecular dynamics simulation. *J. Mol. Liq.* **2019**, *290*, No. 111183.
(78) Speight, J. G. *The chemistry and technology of petroleum*; CRC Press: Boca Raton, FL, 2014.
(79) Mehana, M.; El-monier, I. Shale characteristics impact on Nuclear Magnetic Resonance (NMR) fluid typing methods and correlations. *Petroleum* **2016**, *2*, 138−147.
(80) Zhang, P.; Lu, S.; Li, J.; Chang, X. 1D and 2D Nuclear magnetic resonance (NMR) relaxation behaviors of protons in clay, kerogen and oil-bearing shale rocks. *Mar. Pet. Geol.* **2020**, *114*, No. 104210.
(81) Huang, H.; Li, R.; Chen, W.; Chen, L.; Jiang, Z.; Xiong, F.; Guan, W.; Zhang, S.; Tian, B. Revisiting movable fluid space in tight fine-grained reservoirs: A case study from Shahejie shale in the Bohai Bay Basin, NE China. *J. Pet. Sci. Eng.* **2021**, *207*, No. 109170.
(82) Fleury, M.; Romero-Sarmiento, M. Characterization of shales using T1−T2 NMR maps. *J. Pet. Sci. Eng.* **2016**, *137*, 55−62.
(83) Khatibi, S.; Ostadhassan, M.; Xie, Z. H.; Gentzis, T.; Bubach, B.; Gan, Z.; Carvajal-Ortiz, H. NMR relaxometry a new approach to detect geochemical properties of organic matter in tight shales. *Fuel* **2019**, *235*, 167−177.
(84) Qu, Y.; Sun, W.; Tao, R.; Luo, B.; Chen, L.; Ren, D. Pore−throat structure and fractal characteristics of tight sandstones in Yanchang Formation, Ordos Basin. *Mar. Pet. Geol.* **2020**, *120*, No. 104573.
(85) Wu, Y.; Liu, C.; Ouyang, S.; Luo, B.; Zhao, D.; Sun, W.; Awan, R. S.; Lu, Z.; Li, G.; Zang, Q. Investigation of pore-throat structure and fractal characteristics of tight sandstones using HPMI, CRMI, and NMR methods: A case study of the lower Shihezi Formation in the Sulige area, Ordos Basin. *J. Pet. Sci. Eng.* **2022**, *210*, No. 110053.
(86) Gentzis, T.; Carvajal-Ortiz, H.; Harry Xie, Z.; Hackley, P. C.; Fowler, H. An integrated geochemical, spectroscopic, and petrographic approach to examining the producibility of hydrocarbons from liquids-rich unconventional formations. *Fuel* **2021**, *298*, No. 120357.
(87) Tissot, B. P.; Welte, D. H. *Petroleum Formation and Occurrence*; Springer-Verla: New York, 1984; p 699.
(88) Wang, X. Z.; Song, Y. T.; Wang, X. J. *Petroleum generation and expulsion physical simulation: Method, mechanism and application*; China University of Petroleum Press: China, 1996, p 160.
(89) Li, Z.; Zou, Y.-R.; Xu, X.-Y.; Sun, J.-N.; Li, M.; Peng, P. A. Adsorption of mudstone source rock for shale oil − Experiments, model and a case study. *Org. Geochem.* **2016**, *92*, 55−62.
(90) Hu, T.; Pang, X.-Q.; Jiang, F.-J.; Wang, Q.-F.; Wu, G.-Y.; Liu, X.-H.; Jiang, S.; Li, C.-R.; Xu, T.-W.; Chen, Y.-Y. Key factors controlling shale oil enrichment in saline lacustrine rift basin: implications from two shale oil wells in Dongpu Depression, Bohai Bay Basin. *Pet. Sci.* **2021**, *18*, 687−711.
(91) Hu, T.; Pang, X.; Jiang, S.; Wang, Q.; Zheng, X.; Ding, X.; Zhao, Y.; Zhu, C.; Li, H. Oil content evaluation of lacustrine organic-rich shale with strong heterogeneity: A case study of the Middle Permian Lucaogou Formation in Jimusaer Sag, Junggar Basin, NW China. *Fuel* **2018**, *221*, 196−205.
(92) Wang, M.; Li, M.; Li, J.-B.; Xu, L.; Zhang, J.-Y.; Zhang, J.-X. The key parameter of shale oil resource evaluation: Oil content. *Pet. Sci.* **2022**, *19*, 1443−1459.
(93) Kuila, U.; McCarty, D. K.; Derkowski, A.; Fischer, T. B.; Topór, T.; Prasad, M. Nano-scale texture and porosity of organic matter and clay minerals in organic-rich mudrocks. *Fuel* **2014**, *135*, 359−373.
(94) Hu, T.; Pang, X.; Jiang, F.; Zhang, C.; Wu, G.; Hu, M.; Jiang, L.; Wang, Q.; Xu, T.; Hu, Y.; Jiang, S.; Wang, W.; Li, M. Dynamic continuous hydrocarbon accumulation (DCHA): Existing theories and a new unified accumulation model. *Earth-Sci. Rev.* **2022**, *232*, No. 104109.

https://doi.org/10.1021/acs.energyfuels.2c02222
Energy Fuels 2022, 36, 10920−10933